A Journal of the Gesellschaft Deutscher Chemiker

Angewandte International Edition GDCh Chemie

www.angewandte.org

Accepted Article

Title: A Durable Nickel Single-Atom Catalyst for Hydrogenation Reactions and Cellulose Valorization under Harsh Conditions

Authors: Wengang Liu, Yinjuan Chen, Haifeng Qi, Leilei Zhang, Wensheng Yan, Xiaoyan Liu, Xiaofeng Yang, Shu Miao, Wentao Wang, Chenguang Liu, Aiqin Wang, Jun Li, and Tao Zhang

To be cited as: *Angew. Chem. Int. Ed.* 10.1002/anie.201802231
Angew. Chem. 10.1002/ange.201802231

Link to VoR: http://dx.doi.org/10.1002/anie.201802231
http://dx.doi.org/10.1002/ange.201802231

WILEY-VCH

10.1002/anie.201802231

WILEY-VCH

A Durable Nickel Single-Atom Catalyst for Hydrogenation Reactions and Cellulose Valorization under Harsh Conditions

Wengang Liu,[+] Yinjuan Chen,[+] Haifeng Qi,[+] Leilei Zhang, Wensheng Yan, Xiaoyan Liu, Xiaofeng Yang, Shu Miao, Wentao Wang, Chenguang Liu, Aiqin Wang,* Jun Li,* Tao Zhang

Abstract: Hydrothermally stable and acid-resistant nickel catalysts are highly desired in industrially important hydrogenation reactions. Yet, such catalyst remains absent due to the inherent vulnerability of nickel under acidic reaction media. In this work, we have developed an ultra-durable Ni−N−C single-atom catalyst (SAC) that possesses a remarkable Ni content (7.5 wt%) required for practical usage. This SAC shows not only high activities for hydrogenation of various unsaturated substrates but also unprecedented durability for the one-pot conversion of cellulose under very harsh conditions (245 ^{o}C, 60 bar H_2, presence of tungstic acid in hot water). Using integrated spectroscopy characterization and computational modeling, we have identified the active site structure as (Ni−N4)⋯N, where significantly distorted octahedral coordination and pyridinic N constitute a frustrated Lewis pair for the heterolytic dissociation of dihydrogen, and the robust covalent chemical bonding between Ni and N atoms accounts for its ultrastability.

Biomass, as the most abundant renewable carbon source on the earth, is being explored as an alternative feedstock for production of liquid fuels and chemicals to reduce CO_2 emissions.[1] Different from the traditional petroleum chemical processes that are mainly operated in gas phase, the highly functionalized feature of biomass molecules (O/C ratio as high as 1.0) necessitates the chemical transformations in liquid phase and often at harsh reaction conditions,[2] e.g., strong acid/basic media, high temperature and pressures. Such tough reaction environment raises a significant challenge for the catalyst durability. For example, nickel catalysts were reported to be highly active in the hydrogen-involved biomass conversion reactions such as hydrogenation,[3] hydrogenolysis[4] and hydrodeoxygenation reactions,[5] and nickel would be a favorable choice to noble metals due to its low cost, earth abundance and considerable activity. Unfortunately, most of the nickel catalysts cannot survive under acidic reaction media; the inherent dissolution of low valence state $Ni^0/Ni^{\delta+}$ species in acids will result in leaching and aggregation of catalytically active Ni species, thus significant loss of activity.[6] This vulnerability of nickel catalysts has become a vast barrier for practical applications in biomass transformations. Therefore, it is keenly desired to develop a robust and acid-resistant Ni catalyst for hydrogen-assisted biomass valorizations.

Enormous efforts were made towards improving the stability of Ni catalysts, including encapsulating Ni nanoparticles (NPs) with a porous carbon layer or a carbon nitride layer,[7] as well as alloying with a noble metal.[8] However, physical isolation by an inert layer will cause mass transfer limitations in treating bulky biomass molecules, and the addition of a noble metal can only alleviate the leaching of nickel to a certain extent. Interestingly, single-atom catalysis offers a new strategy to fabricate highly stable active center.[9] The recently developed M-N-C (M refers to transition metals typically like Fe, Co, Ni) single-atom catalysts (SACs) with M bonding strongly with the surrounding N atoms have shown promising performances in various electrochemical reactions[10] as well as organic synthesis.[11] Benefited from the strong covalent chemical bonding between M and N atoms, the M-N-C SACs might be resistant against acid leaching and heat-induced aggregation. Indeed, as shown in our previous work about Fe-N-C and Co-N-C SACs prepared with pyrolysis of N-containing precursors followed by acid etching, the survived Fe and Co atoms after the acid etching remain quite stable during reduction and oxidation reactions.[12] Compared to Fe and Co, Ni tends to have a higher intrinsic activity for hydrogen activation, but the synthesis of Ni-N-C SACs with a practically required Ni loading (e.g., ~10%) is yet to be achieved. Very recently, a few Ni-N-C SACs targeted to electrochemical reactions have been reported although the low Ni loadings (1~2 wt%) preclude practical hydrogenation reactions for biomass valorization.[11a, 11b, 13]

Herein, we report the first synthesis of high-loading Ni-N-C SAC (Ni content 7.5 wt%) and its application for the reaction of cellulose conversion to important polyols (ethylene glycol and acetol). In contrast to the poor stability of Ni NPs supported on active carbon (Ni/AC), the Ni-N-C SAC exhibits unprecedentedly durability under very harsh reaction conditions (245 ^{o}C, 60 bar H_2, presence of tungstic acid in hot water) and it can be reused for at least 7 times without any deactivation or single atom aggregation. Extensive experimental characterizations in conjunction with theoretical studies revealed the active-center structure of (Ni−N4)⋯N and an unusual heterolytic dihydrogen activation mode on a frustrated Lewis pair (FLP) site constituted by isolated Ni cation and the adjacent non-coordinated pyridinic N atom.

To prepare the Ni−N−C SAC, a $Ni(phen)_3$ complex precursor was first dispersed on MgO and then the mixture was submitted to pyrolysis at 600 ^{o}C in N_2 for 2 h, after which the

[☆] W. Liu,[+] H. Qi,[+] L. Zhang, X. Liu, X. Yang, S. Miao, W. Wang, Prof. Dr. A. Wang, Prof. Dr. T. Zhang
State Key Laboratory of Catalysis, and Collaborative Innovation Center of Chemistry for Energy Materials, Dalian Institute of Chemical Physics, Chinese Academy of Sciences
457 ZhongShan Road, Dalian, 116023, China
E-mail: aqwang@dicp.ac.cn
W.Liu; H. Qi
University of Chinese Academy of Sciences, Beijing, 100049, China
Y. Chen,[+] Prof. Dr. Jun Li
Key Laboratory of Organic Optoelectronics & Molecular Engineering of the Ministry of Education, Department of Chemistry, Tsinghua University, Beijing 100084 (China)
E-mail: junli@tsinghua.edu.cn
Y. Chen[+], Chenguang Liu
State Key Laboratory of Heavy Oil Processing, College of Chemical Engineering, China University of Petroleum (East China), Qingdao, Shandong, 266580, China
W. Yan
National Synchrotron Radiation Laboratory, University of Science and Technology of China
Hefei, 230029, China
[+] †These authors contributed equally to this work.

Supporting information for this article is given via a link at the end of the document.

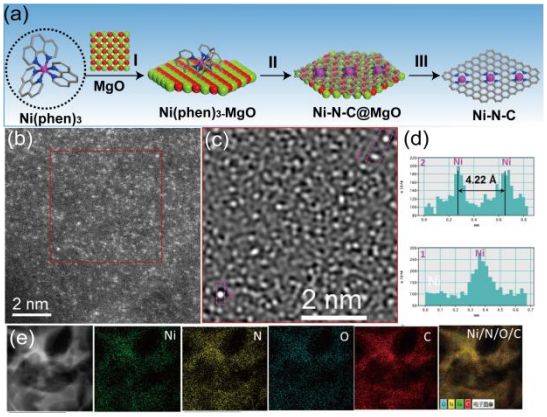

Figure 1. (a) Schematic illustration for preparation of Ni−N−C catalyst; (b) HAADF-STEM image and (c) Fast Fourier transform; (d) Intensity profiles along the lines at positions 1 and 2 in the HAADF-STEM image (c); (e) Elemental mapping of Ni/N/O/C in Ni−N−C catalyst. The white dots in (b, c) are Ni single atoms.

MgO support was removed by acid etching (Figure 1a, more details in supporting information). ICP analysis revealed that the Ni loading was 7.5 wt%, which was several times higher than those of the Ni-N-C SACs prepared by other techniques. [11a, 11b, 13] However, no any Ni or Ni oxide peaks were present in XRD or Raman spectra of the Ni-N-C samples (Figures S1, S2), indicating that the Ni species is highly dispersed.[14] On the other hand, the pyrolysis temperature imposed a significant effect on both the textural properties and the dispersion of Ni species. The BET surface areas reached the highest (500 m^2/g) at 600 ^oC and then decreased markedly to 376 m^2/g at 700 ^oC, indicating the loss of pores due to structural collapse at higher temperatures (Figure S3). This phenomenon, however, was not observed for either Fe-N-C or Co-N-C materials prepared with a similar procedure,[12] implying that the metal species participated in and probably catalyzed the carbonization process. If Ni NPs were formed at 700 ^oC, they would catalyze the methanation of carbon and then resulted in collapse of porous structure. This speculation was confirmed by low-magnification STEM images (Figure S4). For both the Ni-N-C-500 and Ni-N-C-600 samples we did not observe any metal particles. In contrast, Ni particles with sizes of 10-20 nm were clearly observed in the Ni-N-C-700 sample, demonstrating that higher pyrolysis temperature led to considerable aggregation of Ni species. To identify the invisible Ni species in the Ni-N-C-600 sample, we resorted to aberration-corrected subångström-resolution HAADF-STEM technique. As shown in Figure 1b and Figure S5, a high density of Ni single atoms (1.6 Ni atoms/nm^2) were uniformly dispersed in the Ni−N−C-600 sample, and the intensity profiles along the lines at position 1 and 2 (Figure 1c, d) further confirmed that the white dots in Figure 1b are individual Ni atoms. The EDX analysis attached to electron microscope revealed a Ni content of 6.55 wt% (Figure S6), which was close to the value determined by ICP. The elemental mapping showed totally overlapping images of Ni, C, O and N (Figure 1e), suggesting that single atoms of Ni might be chemically bonded with N, C or O.

The chemical states of Ni, N and C in the Ni−N−C sample were probed with XPS (Figure S7). The Ni 2*p* spectra showed two peaks at binding energies of 855.3 eV ($2p_{3/2}$) and 872.7 eV ($2p_{1/2}$), suggesting that Ni single atoms are in a high oxidation state (between Ni^{II} and Ni^{III}).[11b] The N 1*s* spectrum could be deconvoluted into three peaks centered at 399.0, 400.9, and 405.9 eV, which were corresponding to pyridinic N, graphitic N, and N-oxide (N^+-O^-), respectively.[15] The relatively high percentage of pyridinic N (72.2%) could justify the high loading of Ni single atoms since the pyridinic N is generally believed to serve as the coordinating sites for transition metal species.[12] The atomic ratio of pyridinic N to Ni, determined by XPS, was 4.4, suggesting that each Ni atom is coordinated with four or five pyridinic N atoms. This will be verified by the following X-ray absorption spectroscopy characterizations.

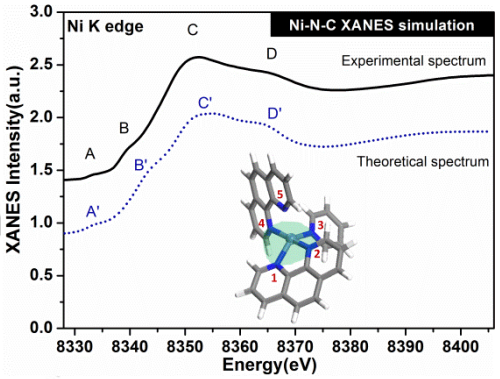

Figure 2. Comparison of experimental and calculated XANES spectra of the Ni-N-C-600, and the inset shows the structure model of Ni-N5.

The structure of the Ni-N-C SAC was resolved by X-ray absorption near-edge structure (XANES) and extended X-ray absorption fine structure (EXAFS) spectroscopy at the Ni K-edge. As shown in Figure S8, the XANES spectra of the three Ni−N−C samples show similar features that are quite different from Ni foil, Ni_2O_3 and Ni(II)Pc. The E_0 values (the first inflection point on the edge; the higher E_0, the higher oxidation state, see Table S1) followed the order of Ni foil < Ni-N-C-700 < Ni(II)Pc < Ni-N-C-600 < Ni-N-C-500 < Ni_2O_3 (inset of Figure S8), confirming that the Ni single atoms in the Ni-N-C-600 are between Ni^{II} and Ni^{III}, which is in good agreement with the XPS result. Moreover, the XANES spectrum of the Ni−N−C-600 catalyst presents four distinct features (Figure 2, black line): (i) peak A, pre-edge at 8333 eV; (ii) peak B, pre-edge at 8339 eV; (iii) peak C, absorption edge at 8351 eV; (iv) peak D, post-edge at 8366 eV. The first pre-edge peak A can be attributed to the 1*s*→3*d* electronic transition of Ni cations in an octahedral symmetry,[16] although this transition is generally forbidden in octahedral ligand field due to orbital symmetry mismatch. Only slight (*p*-*d*) orbital mixing in distorted local symmetry can give some probability for the 1*s*→3*d* transitions.[16b] Therefore, we speculate that the Ni single atoms in the Ni-N-C-600 might be located in a distorted octahedral coordination geometry. The second pre-edge peak B is due to the 1*s*→4p_z electronic transition, which is often regarded as the fingerprint of square-planar M−N4 moiety.[12a, 17] Compared to Ni(II)Pc (Figure S8), the remarkably weakened peak B of the Ni-N-C-600 indicates also a significantly distorted Ni-N4 structure. In addition, the main peak C at the absorption edge corresponds to transition from 1*s* to 4*p* continuum states and the fourth peak D occurring ~15 eV above the main peak C is due to the multiple scattering.[16a, 18]

Based on these features, we constructed using density functional theory (DFT) calculations various models with different coordination geometries (planar or nonplanar, nitrogen or oxygen atoms, distinct Ni−N4, Ni−N5 and Ni−N6 structures). For computational details see supporting information. We calculated XANES spectrum of each model and compared it with the experimental spectrum of the Ni−N−C-600 catalyst (Figure S9). It turned out that the theoretical XANES spectrum of (Ni−N4)---N configuration (dotted line and inset in Figure 2) could perfectly reproduce the main features of the experimental spectrum of Ni−N−C-600 catalyst. In this model, the Ni center atom is coordinated with four pyridinic N atoms (Ni−$N_1N_2N_3N_4$) to form a significantly distorted quasi-planar Ni-N4 structure, while the fifth pyridinic N atom coordinates very weakly to the centre Ni atom in the perpendicular direction. As a result, the whole Ni-N5 structure can be viewed as substantially distorted octahedral coordination geometry with a ligand-missing. The good agreement between this XANES-optimized Ni-N5 structure and the XPS-determined pyridinic N/Ni atomic ratio (4.4) implies the homogeneity of the structure throughout the catalyst.

The above structure was corroborated with EXAFS result at the Ni K-edge. As shown in Figure S10, the Fourier transformed k^2-weighted EXAFS spectrum of the Ni−N−C-600 presents only one prominent peak at ca. 1.40 Å, similar to the feature of Ni(II)Pc. This peak should be attributed to the coordination between Ni and light C/N elements. The absence of Ni-Ni bond agrees with HAADF-STEM result while the fitting result of the EXAFS data showed two distinct Ni-N coordination shells, with a coordination number of 3.4 and 1.7 at a distance of 1.90 and 2.14 Å (Figure S11, S12 and Table S2), respectively. This result agrees well with the DFT and XANES calculation result (Table S3) within the error limit.

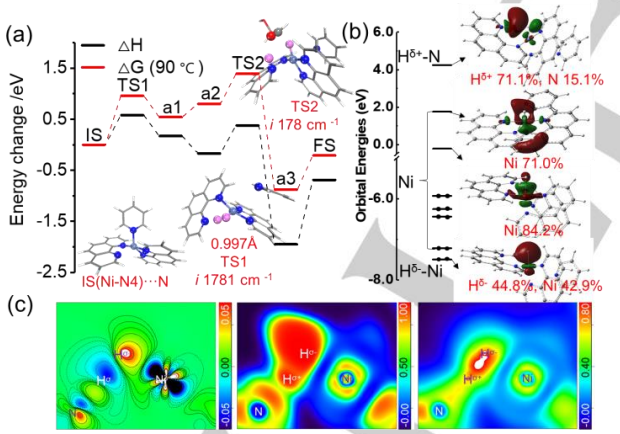

Figure 3. (a) The proposed H_2 activation and glycolaldehyde hydrogenation energy change profile on Ni-N-C-600 catalyst. (b) The energy level of H_2 heterolytic splitting species a1 and localized molecular orbitals (LMOs, see also Figure S13a). (c) Maps of electron density difference, electron localization function (ELF), and localized orbital locator (LOL) of TS1 (from left to right, relevant maps of a1 see Figure S13b).

Such a well-defined Ni-N5 structure is able to activate hydrogen in spite of relatively high oxidation state of central Ni atoms. The DFT calculations show that H_2 molecule can be activated heterolytically. When dihydrogen molecule approaches Ni centre, it is activated via the interaction with Ni and the adjacent pyridinic N atoms. As a result, the H_2 inserts into Ni-N_5 with the H-H bond elongated by 0.237 Å (from 0.760 Å in gas phase H_2 to 0.997 Å in TS1) and the weak Ni-N_3 bond is cleaved (Figure 3a, TS1). It can be viewed as the coordination exchange of the pyridine ligand and hydrogen atom during H_2 activation. The activation barrier for this step is 0.58 eV (△H), which is 0.87 eV lower than that on Au(111) surface.[19] The electron density difference of TS1 (Figure 3c) shows a significant electron density decrease on $H^{\delta+}$ and an increase on $H^{\delta-}$. From the ELF and LOL maps the covalent interaction between N and $H^{\delta+}$ is clearly seen, and the high localization of electron density around $H^{\delta-}$ and delocalization between $H^{\delta-}$ and Ni are also observed. Consequently, the H_2 molecule is heterolytically dissociated to form a meta-stable $H^{\delta+}$-N and $H^{\delta-}$-Ni configuration (Figure 3b and Figure S13). The localized molecular orbitals (LMOs) and the localized orbital bonding analysis (LOBA) clearly show the oxidation state of each split H atoms and Ni center (Figure 3b), $H^{\delta+}$ +1, $H^{\delta-}$ -1 and Ni(II).[20] Such a heterolytic dissociation manner is reminiscent of the FLP in homogeneous catalysis, which can perform well the activation of dihydrogen in a similar way.[21] Indeed, the Ni-N5 structure possesses both Lewis acid and basic sites as revealed by CO_2-TPD and NH_3-TPD process (Figure S14). It can be anticipated that our Ni-N-C catalyst with well-defined Ni-N5 structure will be active in a series of hydrogenation reactions.

As expected, the catalyst showed excellent activity for the hydrogenations of various biomass-bearing unsaturated groups including nitroarenes (-NO_2), aldehyde (-C=O), styrene (-C=C-), phenylacetylene (-C≡C-) and quinline (-C=N-). Remarkably, nearly 100% yields of the corresponding products were achieved under mild conditions (Figure S15). To identify the FLP mechanism, we made two control experiments. First, we deliberately added pyrrole molecule as a Lewis acid into the reaction system of nitrobenzene hydrogenation, and found that the yield of aniline drastically declined from 99.0% to 39.4% (Figure S16), suggesting that Lewis basic sites are necessary for the reaction. Second, we added SCN^- ion to poison the Ni cations (Lewis acid sites) and the yield decreased to 11.1%. Based on these control experiments, we propose that the Ni cations (Lewis acid sites) and the neighbouring non-coordinated pyridinic N atoms (Lewis basic sites) constitute a FLP that act as the active sites for hydrogenations. This FLP mechanism is proved by DFT calculations. As shown in Figure 3a and Figure S17, upon the formation of $H^{\delta+}$ and $H^{\delta-}$ via FLP, the hydrogenation of unsaturated substrate could proceed facilely (from a2 to FS in Figure 3a). For example, for the glycolaldehyde hydrogenation, our DFT calculation revealed that an energy barrier of only 0.55 eV is required (Figure 3a, Figure S17 and Table S4), which means that the hydrogenation can proceed even at room temperature.

Not only with high activity for hydrogenation of a variety of unsaturated substrates, the Ni-N-C SACs also possess outstanding stability inherited from the strong covalent bonding between Ni and N atoms. In fact, the high temperature pyrolysis as well as the subsequent acid-etching processing during the synthesis of Ni-N-C SACs has already indicated that the Ni-N_x sites are highly resistant against sintering and acid-leaching. To study the stability of the Ni-N_x during hydrogenation reactions,

here we apply the catalyst to the one-pot conversion of cellulose to ethylene glycol, which is a key reaction in the valorization of renewable lignocellulose.[1a, 6, 22] To degrade the recalcitrant cellulose, a binary catalyst composed of tungstic acid and Ni-N-C-600 was used, in which the tungstic acid promotes C-C cleavage of the cellulose-derived sugars via a retro-aldol pathway while the Ni-N-C-600 catalyzes the hydrogenation of aldehyde intermediates (Figure S18).[1a]

Based on our earlier studies,[1a, 6, 22] cellulose hydrolysis as well as the C-C cleavage reaction had a high activation energy and thus required a very harsh reaction condition (245 °C, 60 bar H_2, stongly acidic hydrothermal conditions). Cogently, most of the base metal catalysts could not survive under such severe conditions. As expected, our Ni-N-C-600 catalyst shows promising activity (Figure 4a, left), with cellulose completely converted and the main products as EG (36.8%) and acetol (17.4%). The formation of acetol suggests the occurrence of isomerization of glucose to fructose, which is usually catalyzed by Lewis acid or basic sites (Figure S19), again proving the FLP feature of the Ni-N-C-600 catalyst. Furthermore, the Ni-N-C-600 catalyst has unprecedented durability under aforementioned harsh reaction conditions; the total yield of EG and acetol only has a slight decrease from 54.2% in the first run to the 47.4% in the 7th run. Further inspection of the reused catalyst reveals that this slight loss is not caused by the catalyst deactivation; instead, it results from the decreased feed of the Ni-N-C-600 catalyst during reuse test. We note that approximately 20% tungsten is deposited on the Ni-N-C-600 catalyst after seven reuses, which is not considered during the reuse test.

In remarkable contrast to the excellent stability of the Ni-N-C SAC, the Ni NPs supported on active carbon (Ni/AC) lost half of the initial activity in the second run (Figure 4a, right) although the initial activity of the Ni/AC was much higher (TOF 663.9 h^{-1} for glycolaldehyde hydrogenation on Ni/AC while 57.3 h^{-1} for Ni-N-C). The characterizations of the reused catalysts show that the Ni-N-C-600 structure remains intact; single atoms of Ni are still highly dispersed and no aggregation is observed (Figure 4b, Figure S20a). Morevoer, the XPS, EXAFS and XANES spectra of the Ni-N-C-600 catalyst keep unchanged before and after the reaction (Figure S21, S22), indicating that the partially reduced Ni species can be completely restored to the high oxidation state and stay bonded to N atoms. In contrast, significant sintering of Ni NPs ocurs as a result of leaching and redeposition of active Ni species (Figure 4c, Figure S20b), which is ubiquitous when nickel metal catalyst is used at acidic or hydrothermal reaction conditions.

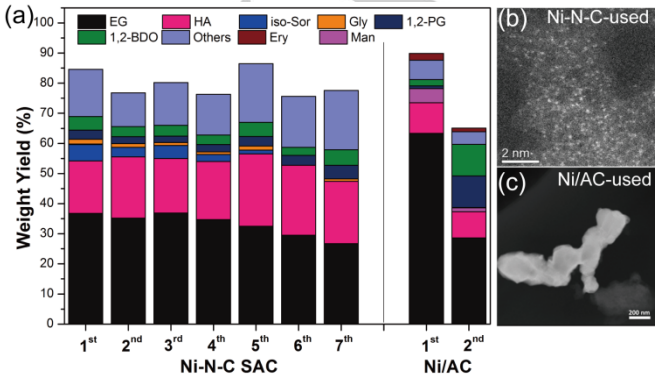

Figure 4. (a) Durability of the Ni−N−C-600 in comparison with Ni/AC for the one-pot conversion of cellulose. Reaction condition: 0.3 g cellulose, 50 mg catalyst, 30 mg tungstic acid and 30 mL water in 100 mL autoclave, 245 °C, 6.0 MPa H_2, 1 h 45 min, 1000 rpm. (b, c) HAADF-STEM images of the reused Ni-N-C-600 and Ni/AC catalysts. EG (black): ethylene glycol; HA (pink): Hydroxyacetone; Iso-sor (blue): Iso-sorbitol; Man (magenta): mannitol; Gly (orange): glycerol; 1,2-PG (navy): 1,2-propylene glycol; 1,2-BDO (olive): 1,2-Butanediol; others (light violet); Ery (wine): erythritol.

In summary, we have synthesized a high-loading Ni−N−C single-atom catalyst, which not only is active for hydrogenation of various unsaturated substrates, but also manifests extraordinary durability for cellulose conversion under harsh reaction conditions. The high activity and ultrastability arise from the significantly distorted (Ni−N4)⋯N structure, in which the isolated nickel cation and the adjacent non-coordinated pyridinic N atoms constitute FLP sites for heterolytic dissociation of dihydrogen. The atomic resolution of the active sites will help to design and explore more efficient and robust catalysts towards biomass and other energy-related reactions.

Acknowledgements

The authors are grateful to the National Natural Science Foundation of China (21690080, 21690084, 21673228, 21721004, 21590792, 91645203,11435012) and the Strategic Priority Research Program of the Chinese Academy of Sciences (XDB17020100), the National Key Projects for Fundamental Research and Development of China (2016YFA0202801), the Fundamental Research Funds for the Central Universities (15CX06037A), and the BL 14W beamline at the Shanghai Synchrotron Radiation Facility (SSRF). The calculations were performed using supercomputers at Tsinghua National Laboratory for Information Science and Technology, and the Computational Chemistry Laboratory (Xuetang) of the Department of Chemistry, Tsinghua University.

Keywords: Ni−N−C • Single-atom catalyst • active site • XANES simulation • biomass conversion

[1] a) A. Wang, T. Zhang, *Acc. Chem. Res.* **2012**, *46*, 1377–1386; b) M. Besson, P. Gallezot, C. Pinel, *Chem. Rev.* **2014**, *114*, 1827-1870.
[2] a) W. Deng, Q. Zhang, Y. Wang, *J. Energy Chem.* **2015**, *24*, 595-607; b) Y. Liu, C. Luo, H. Liu, *Angew. Chem., Int. Ed.* **2012**, *51*, 3249-3253; *Angew. Chem.* **2012**, 124, 3303-3307; c) Y. Zhang, A. Wang, T. Zhang, *Chem. Commun.* **2010**, *46*, 862-864..
[3] a) M. Sudhakar, V. V. Kumar, G. Naresh, M. L. Kantam, S. K. Bhargava, A. Venugopal, *Appl. Catal., B* **2016**, *180*, 113-120; b) Z. Tai, J. Zhang, A. Wang, J. Pang, M. Zheng, T. Zhang, *ChemSusChem* **2013**, *6*, 652-658.
[4] a) Q. Zhang, T. Jiang, B. Li, T. Wang, X. Zhang, Q. Zhang, L. Ma, *ChemCatChem* **2012**, *4*, 1084-1087; b) D. Scholz, C. Aellig, I. Hermans, *ChemSusChem* **2014**, *7*, 268-275.
[5] a) Y. Nakagawa, S. Liu, M. Tamura, K. Tomishige, *ChemSusChem* **2015**, *8*, 1114-1132; c) J. Lee, Y. T. Kim, G. W. Huber, *Green Chem.* **2014**, *16*, 708.
[6] N. Ji, T. Zhang, M. Zheng, A. Wang, H. Wang, X. Wang, J. G. Chen, *Angew. Chem., Int. Ed.* **2008**, *47*, 8510-8513; *Angew. Chem*. **2008**, 120, 8638-8641 .
[7] a) H. Xiong, T. J. Schwartz, N. I. Andersen, J. A. Dumesic, A. K. Datye, *Angew. Chem., Int. Ed.* **2015**, *54*, 7939-7943; *Angew. Chem.* **2015**, 127, 8050-8054; b) T. Fu, M. Wang, W. Cai, Y. Cui, F. Gao, L. Peng, W. Chen, W. Ding, *ACS Catal.* **2014**, *4*, 2536-2543.
[8] S. De, J. Zhang, R. Luque, N. Yan, *Energy Environ. Sci.* **2016**, *9*, 3314-3347.

[9] a) B. Qiao, A. Wang, X. Yang, L. Allard, Z. Jiang, Y. Cui, J. Liu, J. Li, T. Zhang *Nature Chem*., **2011**, 3, 634−641; b) X. Yang, A. Wang, B. Qiao, J. Li, J. Liu, T. Zhang, *Acc. Chem. Res.*, **2013**, 46, 1740-1748; c) J. Jones, H. Xiong, A.T. DeLaRiva, E.J. Peterson, H. Pham, S. R. Challa, G. Qi, S. Oh, M. H. Wiebenga, X. I. P. Hernández, Y. Wang, A. K. Datye, *Science*, **2016**, 353, 150-154.

[10] a) Y. Chen, S. Ji, Y. Wang, J. Dong, W. Chen, Z. Li, R. Shen, L. Zheng, Z. Zhuang, D. Wang, Y. Li, *Angew. Chem., Int. Ed.* **2017**, *56*, 6937–6941; *Angew. Chem.* **2017**, 129, 7041-7045; b) P. Chen, T. Zhou, L. Xing, K. Xu, Y. Tong, H. Xie, L. Zhang, W. Yan, W. Chu, C. Wu, Y. Xie, *Angew. Chem., Int. Ed.* **2016**, *56*, 610-614; *Angew. Chem.* **2017**, 129, 625-629.

[11] a) X. Li, W. Bi, M. Chen, Y. Sun, H. Ju, W. Yan, J. Zhu, X. Wu, W. Chu, C. Wu, Y. Xie, *J. Am. Chem. Soc.* **2017**, *139*, 14889-14892; b) C. Zhao, X. Dai, T. Yao, W. Chen, X. Wang, J. Wang, J. Yang, S. Wei, Y. Wu, Y. Li, *J. Am. Chem. Soc.* **2017**, *139*, 8078–8081; c) L. Zhang, A. Wang, W. Wang, Y. Huang, X. Liu, S. Miao, J. Liu, T. Zhang, *ACS Catal.* **2015**, *5*, 6563-6572.

[12] a) W. Liu, L. Zhang, X. Liu, X. Liu, X. Yang, S. Miao, W. Wang, A. Wang, T. Zhang, *J. Am. Chem. Soc.* **2017**, *139*, 10790-10798; b) W. Liu, L. Zhang, W. Yan, X. Liu, X. Yang, S. Miao, W. Wang, A. Wang, T. Zhang, *Chem. Sci.* **2016**, *7*, 5758-5764.

[13] a) H. J. Qiu, Y. Ito, W. Cong, Y. Tan, P. Liu, A. Hirata, T. Fujita, Z. Tang, M. Chen, *Angew. Chem., Int. Ed.* **2015**, *54*, 14031-14035; *Angew. Chem.* **2015**, 127, 14237-14241; b) L. Fan, P. F. Liu, X. Yan, L. Gu, Z. Z. Yang, H. G. Yang, S. Qiu, X. Yao, *Nat. Commun.* **2016**, *7*, 10667.

[14] a) L. Chen, L. Zhang, Z. Chen, H. Liu, R. Luque, Y. Li, *Chem. Sci.* **2016**, *7*, 6015-6020; b) Z. Han, S. Li, F. Jiang, T. Wang, X. Ma, J. Gong, *Nanoscale* 2014, 6, 10000-10008.

[15] L. He, F. Weniger, H. Neumann, M. Beller, *Angew. Chem., Int. Ed.* **2016**, *55*, 12582-12594; *Angew. Chem.* **2016**, 128, 12770-12783.

[16] a) T. Ikuno, J. Zheng, A. Vjunov, M. Sanchez-Sanchez, M. A. Ortuno, D. R. Pahls, J. L. Fulton, D. M. Camaioni, Z. Li, D. Ray, B. L. Mehdi, N. D. Browning, O. K. Farha, J. T. Hupp, C. J. Cramer, L. Gagliardi, J. A. Lercher, *J. Am. Chem. Soc.* **2017**, *139*, 10294–10301; b) A. Sharma, M. Varshney, H. J. Shin, B.-H. Lee, K. H. Chae, S. O. Won, *Mater. Chem. Phys.* **2017**, *191*, 129-144.

[17] A. Zitolo, V. Goellner, V. Armel, M. T. Sougrati, T. Mineva, L. Stievano, E. Fonda, F. Jaouen, *Nat. Mater.* **2015**, *14*, 937-942.

[18] Y. Cao, S. Chen, Q. Luo, H. Yan, Y. Lin, W. Liu, L. Cao, J. Lu, J. Yang, T. Yao, S. Wei, *Angew. Chem., Int. Ed.* **2017**, *56*, 12191–12196; *Angew. Chem.* **2017**, 129, 12359-12364.

[19] J. L. Fiorio, N. López, L. M. Rossi, *ACS Catal*. **2017**, *7*, 2973-2980.

[20] A. J. W. Thom, E. J. Sundstrom, M. Head-Gordon, *Phys. Chem. Chem. Phys.* **2009**, *11*, 11297-11304.

[21] a) D. W. Stephan, *J. Am. Chem. Soc.* **2015**, *137*, 10018-10032; b) S. Zhang, Z. Q. Huang, Y. Ma, W. Gao, J. Li, F. Cao, L. Li, C. R. Chang, Y. Qu, *Nat. Commun.* **2017**, *8*, 15266; c) X. Zhao, J. Wang, M. Yang, N. Lei, L. Li, B. Hou, S. Miao, X. Pan, A. Wang, T. Zhang, *ChemSusChem* **2017**, *10*, 819-824; d) Z.Q. Huang, L. P. Liu, S. Qi, S. Zhang, Y. Qu, C. R. Chang, *ACS Catal.* **2018**, 8, 546-554.

[22] G. Xu, A. Wang, J. Pang, X. Zhao, J. Xu, N. Lei, J. Wang, M. Zheng, J. Yin, T. Zhang, *ChemSusChem* **2017**, *10*, 1390-1394.

10.1002/anie.201802231

WILEY-VCH

Entry for the Table of Contents (Please choose one layout)

Layout 1:

COMMUNICATION

A durable and high loading nickel single-atom catalyst is developed for hydrogenation reactions and one-pot conversion of cellulose to ethylene glycol under harsh conditions. The catalyst is featured with a well-defined active site with a significantly distorted (Ni−N4)---N structure, in which the isolated nickel cation and the adjacent non-coordinated pyridinic N atom constitute a Frustrated Lewis Pair for heterolytic dissociation of dihydrogen.

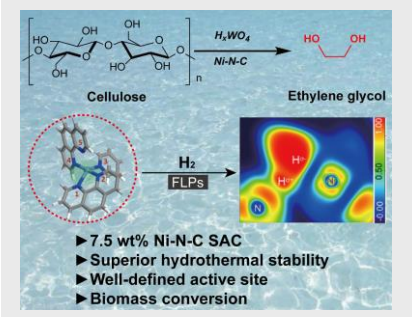

Wengang Liu, Yinjuan Chen, Haifeng Qi, Leilei Zhang, Wensheng Yan, Xiaoyan Liu, Xiaofeng Yang, Shu Miao, Wentao Wang, Chenguang Liu, Aiqin Wang, Jun Li,* Tao Zhang**

Page No. – Page No.

A Durable Nickel Single-Atom Catalyst for Hydrogenation Reactions and Cellulose Valorization under Harsh Conditions